



Red Sea during the Last Glacial Maximum: Implications for sea level reconstruction

E. Biton,¹ H. Gildor,¹ and W. R. Peltier²

Received 13 February 2007; revised 29 July 2007; accepted 30 October 2007; published 19 March 2008.

[1] The Red Sea is connected to the Indian Ocean via a narrow and shallow strait and exhibits a high sensitivity to atmospheric changes and a reduced sea level. We used an ocean general circulation model to investigate the hydrography and circulation in the Red Sea in response to reduced sea level and modified atmospheric conditions occurring during the Last Glacial Maximum (LGM). The model salinity shows high sensitivity to sea level reduction together with a mild atmospheric impact. Sea level reduction affects the stratification and alters the circulation pattern at the Strait of Bab el Mandab, which experiences a transition from a submaximal flow to a maximal flow. The best correlation to reconstructed conditions during LGM exists when the water depth of the Hanish Sill (the shallowest part in the Strait of Bab el Mandab) is 33 ± 10.75 m, which would be affected by a sea level lowering of approximately 105 m. Our results support the reconstructed maximum salinity of around 57 practical salinity units because of a simple model (that takes into account mixing processes along the strait) and comparison of the surface salinity gradient to reconstructions based on isotopic records from sedimentary cores. The salinity and $\delta^{18}\text{O}$ are sensitive to the mixing process at the strait, and the sensitivity increases as the sea level is further reduced. A local relative sea level reduction of approximately 105 m is also in close agreement with the inference of the LGM low stand of the sea at the location of the sill based on the ICE-5G (VM2) model.

Citation: Biton, E., H. Gildor, and W. R. Peltier (2008), Red Sea during the Last Glacial Maximum: Implications for sea level reconstruction, *Paleoceanography*, 23, PA1214, doi:10.1029/2007PA001431.

1. Introduction

[2] We have used an ocean general circulation model (OGCM) and a simple hydraulic control model, which takes into account the effects of the mixing process at the Strait of Bab el Mandab, to investigate the hydrography and circulation in the Red Sea (RS) in response to reduced sea level, variability in the Indian monsoons, and changes in atmospheric temperature and humidity occurring during the Last Glacial Maximum (LGM). In this manuscript we concentrate on the effects of reduced sea level and changes in atmospheric conditions on the salinity and $\delta^{18}\text{O}$ of the RS, and the implications for sea level reconstructions.

[3] Reliable reconstructions of past sea level are crucial for understanding the mechanisms responsible for both glacial-interglacial cycles as well as for climate variability on shorter timescales. Such reconstructions are usually based on records of relative sea level change recorded at a limited number of sites on the Earth's surface, for example, those occupied by coral reefs. Information from such sites is then employed to constrain predictive models which take into account the Earth's rheology, rotation, and shoreline migration patterns to yield predictions of the history of

relative sea level change as a function of geographical location. Present estimates for the ice equivalent eustatic sea level reduction for the LGM interval range between approximately 120 m [Peltier, 2004, 2002; Peltier and Fairbanks, 2006] and approximately 135 m below the present-day global sea level [Yokoyama *et al.*, 2000; Lambeck *et al.*, 2002].

[4] The amount by which sea level is reduced at a given location will not normally be equal to the globally averaged reduction. Estimates of local relative sea level change can be employed to validate and refine models of the global variation of sea level and can be used to distinguish between competing models. Encircled by arid land masses with low precipitation and undergoing one of the highest evaporation rates that has been recorded globally, the properties of the RS are largely controlled by the exchange flow through the Strait of Bab el Mandab and therefore are extremely sensitive to sea level reduction, as previously noted [Siddall *et al.*, 2003; Rohling *et al.*, 1998; Arz *et al.*, 2007, 2003; Thunell *et al.*, 1988].

[5] At present the sill depth is 137 m at its deepest point [Werner and Lange, 1975]. During LGM, reduced sea level leads to reduced exchange flow through the strait, resulting in an increase in the residence time of water within the RS and increased impact of the evaporation process on the RS. Indeed, records from the central RS for the last 380 ka [Hemleben *et al.*, 1996] show a marked shift of 3.5–5.5 parts per thousand (ppt) in $\delta^{18}\text{O}$ between glacial and interglacial conditions, compared with only a 1.2–1.3 ppt shift in other oceans [Fairbanks, 1989]. Such large anoma-

¹Department of Environmental Sciences and Energy Research, Weizmann Institute of Science, Rehovot, Israel.

²Department of Physics, University of Toronto, Toronto, Ontario, Canada.

lies in $\delta^{18}\text{O}$ normally reflect high salinity values. Salinity reconstructions based on sediment cores taken from several places in the RS show salinity values as high as 50.5–57 practical salinity units (psu) [Hemleben *et al.*, 1996; Arz *et al.*, 2003; Geiselhart, 1998; Fenton *et al.*, 2000], 10–17 psu greater than present-day salinity values. Thus during LGM, salinity values exceeded the tolerance of all planktonic foraminifera species, resulting in an “aplanktonic zone” that is recorded in sediment cores taken from the central and northern parts of the RS [Thunell *et al.*, 1988; Fenton *et al.*, 2000; Hemleben *et al.*, 1996], which set a minimum salinity value of 49 psu during that interval of time [Hemleben *et al.*, 1996]. Evidence is also available that suggests the existence of a south-north (S-N) salinity gradient similar to that which exists at present, with maximum values occurring at the northern end of the RS [Fenton *et al.*, 2000]. Although LGM concentrations were lower compared to their modern abundance, foraminifera were found at the southernmost part of the RS, indicating a considerably less hostile environment than that which existed in the basin interior (<45 psu [Fenton *et al.*, 2000]) because of the proximity of the exchange flow to the open Indian Ocean.

[6] In addition to reduced sea level, other factors, such as changes of strength of the Indian monsoon and increased atmosphere aridity, may also contribute to the observed increase in salinity values [Almogi-Labin *et al.*, 1998; Hemleben *et al.*, 1996]. There exists considerable evidence suggesting that significant modifications to the Indian monsoon were also characteristic of the LGM interval; the summer southwest (SW) monsoon was substantially weakened at that time [Anderson and Prell, 1993; Bigg and Jiang, 1993; Sirocko *et al.*, 1993], whereas the winter northeast (NE) monsoons were intensified, as revealed on the basis of alkenone sea surface temperature (SST) records [Ten Haven and Kroon, 1991], pollen records [Van Campo *et al.*, 1982], and intensified dune activities during LGM [Singh *et al.*, 1972; Goudie *et al.*, 1973]. Evidence from the RS itself reveals a similar picture: Rohling [1994] associated a drop of some 50% in ^{18}O enrichment due to evaporation during LGM to the intensified winter monsoons. Fenton *et al.* [2000] suggested a correlation between a northward expansion of the southern RS oxygen minimum zone during LGM and the dominant NE monsoon in the region during that time. The intensified NE monsoon during LGM is also revealed in sediment records in the Gulf of Aden [Almogi-Labin *et al.*, 2000] and the eastern Arabian Sea [Anajali *et al.*, 2005; Banakar *et al.*, 2005].

[7] On the basis of our models, to be discussed in sections 2 and 3, we suggest that the salinity in the RS during LGM was not higher than 57 psu and that local relative sea level was reduced by only ~ 105 m in the Bab el Mandab region, i.e., the water depth at the Hanish Sill (the shallowest part in the Strait of Bab el Mandab) was approximately 35 m. This result agrees with the predicted local LGM lowering of sea level based upon the ICE-5G (VM2) model of Peltier [2004], a model characterized by an ice equivalent eustatic lowering of sea level of 120 m at LGM. If the difference between the local and eustatic lowering of sea level in the model of Lambeck *et al.* [2002] were to be equal to that in the model of Peltier [2004], namely, 15 m, then this model

of Lambeck *et al.* [2002] would predict a local analog sea level in the Strait of Bab el Mandab of 120 m (i.e., 135 m - 15 m). Our results also suggest that mixing processes in the Bab el Mandab region become more significant at very low sea level and significantly affect estimated sea level during the LGM. However, even for a sea level reduction that is less than 100 m, uncertainties in the amount of mixing can introduce large errors in sea level reconstructions. Our models agree with Siddall *et al.* [2004] that the effect of changes in atmospheric conditions on the RS salinity are much weaker than the effect of reduced sea level.

[8] The organization of the article is as follows: Section 2 briefly describes the results of the OGCM in response to sea level reduction and to changes in atmospheric conditions. With the aid of a simple box model which takes into account mixing processes within the strait, we discuss in section 3 the implications of our result on sea level reconstruction and compare them to those obtained using the ICE-5G (VM2) model of Peltier [2004]. We conclude in section 4.

2. OGCM Results

[9] In this work, we employ the oceanic general circulation model developed at the Massachusetts Institute of Technology [Marshall *et al.*, 1997a, 1997b]. The model supports a wide range of parameterizations; in our setting the model solves the hydrostatic primitive equations, including a linear free surface boundary condition and explicit fresh water flux. The model domain includes the whole RS area and part of the Gulf of Aden extending to 45°E . Siddall *et al.* [2002] demonstrate the importance of using a realistic bathymetry at the Strait of Bab el Mandab in order to simulate correctly the exchange flux. The bathymetry in our model is based on 2-minute Worldwide Bathymetry/Topography dataset (ETOPO2) (ETOPO2 data are available at <http://www.ngdc.noaa.gov/mgg/bathymetry/relief.html>.) so the change in the shape of the strait, especially the narrowing with depth, is accurately taken into account.

[10] Assuming the Tiran Strait bathymetry (connecting the Gulf of Eilat to the RS at its northern end) has not changed since the LGM, the Gulf of Eilat was connected to the RS even at times when the sea level was at its minimum. However, the strait was much narrower during LGM than it is today, and the resolution of our grid is too coarse to account for this. We therefore connect the Gulf of Eilat and the RS using a “cross-land” mixing scheme [Griffies *et al.*, 2004], allowing only heat and salt exchange between the two basins in all the numerical experiments that we have performed. Generally speaking, because the volume of the Gulf of Eilat is only 1% of the volume of the RS, we do not expect that it will significantly influence the properties of the RS (which are mainly controlled by the exchange flux at the Strait of Bab el Mandab and the air-sea fluxes in the interior RS). However, as the Gulf of Eilat is one of the sources for the bottom water of the RS (see Plahn *et al.* [2002] and discussion in the supplementary information¹), it

¹Auxiliary materials are available in the HTML. doi:10.1029/2007PA001431.

was included in order to improve the simulations as much as possible. The results for the present-day simulation (PD) control experiment for the Gulf of Eilat as well as for the RS hydrography were in close accord with the observations, suggesting that the connection of the two basins via the “cross-land” mixing scheme has been reasonably represented.

[11] A full surface mixed layer scheme, referred to in the literature as the K-Profile Parameterization scheme, is employed [Large *et al.*, 1994]. Evaporation and surface turbulent flux components such as latent heat, sensible heat, and wind stress (for the prescribed wind components) were calculated in situ by the model on the basis of atmospheric data and using the methodology described by Large and Pond [1982, 1981]. The spatial resolution is 2 minutes across the RS and 5 minutes along its main axis (1 minute is approximately 1.8 km). The water column is resolved by 13 levels in the vertical, with 7 of these layers concentrated in the upper ~200 m in order to capture the complex dynamics of the upper ocean. Further detailed description of the model can be found in the supplementary information.

[12] The model was first run for present-day conditions as a control experiment, and it reproduces rather well the main features of circulation and hydrography of the RS, including the exchange flux at the Strait of Bab el Mandab (supplementary information). Since sea level is a dominant force affecting RS properties, we have conducted three experiments that differ only in their sea level height relative to that assumed in the PD, with a local sea level reduction of 120 m (M120), 105 m (M105), and 90 m (M90). Two more experiments, M120L and M105L (having the same sea level as the M120 and M105 experiments, respectively), were conducted but were under different atmospheric conditions in order to better represent the RS under LGM atmospheric conditions.

2.1. Sea Level Sensitivity Tests

[13] In this section our purpose is to intercompare experiments M120, M105, M90, and PD. We will concentrate on the salinity and briefly discuss the RS response to sea level reduction in terms of the exchange pattern at the Strait of Bab el Mandab. The dominant feature related to reduced sea levels between the experiments is the reduction of the depth at the Strait of Bab el Mandab as the sea level is reduced. There are two more substantial differences between the PD and the reduced sea level experiments: (1) The surface area in the PD experiment is almost twice the area in the other three experiments because of the wide areas of the continental shelves, which dried as the sea level was reduced. (2) The Gulf of Suez is not included as one of the sources of deep water formation (as is prevailing in the PD) in the reduced sea level experiments. The characteristic dimensions of the Strait of Bab el Mandab, as well as the RS surface area, are important, mainly for heat and salt balance within the basin, as can be shown on the basis of the Knudsen formula [Knudsen, 1900]. However, since the atmospheric forcing is the same in all four experiments, several main features characteristic of the PD are preserved in all four experiments (discussed in further detail in the supplementary information), including complex surface dynamics characterized by a series of gyres along the basin,

deep water formation at the north of the basin during winter, and a well-stratified water column during the summer months.

2.2. Exchange Flux With the Indian Ocean

[14] To investigate the differences in the exchange flux between the PD control model and the sea level reduction experiments, we chose the Hanish Sill location, where the exchange flux is controlled. The results of the monthly average fluxes, salinity, temperature, and potential density anomaly at different exchange layers for all experiments are shown in Figure 1. In all cases, the exchange flux is reduced with the reduction in the dimensions of the strait, resulting in an increase of isolation at the basin. All sea level reduction experiments (M120, M105, and M90) exhibit a two-layer exchange flux year round (Figure 1), without a transition to three-layer exchange flux during August–September as in PD (supplementary information, Figure S7). A major seasonal change in the M120 experiment regarding the exchange flux pattern is observed, namely, an exchange flux minimum at winter compared to summer, opposite to the PD circumstance (supplementary information, Figure S7). In M120 there is a high correlation between the exchange flux rate (Figure 1c) and the stratification (which is simply the subtraction between the two layers’ density (Figure 1i, indicated by the dash-dotted line)) at the strait, most likely indicating that stratification is the dominant seasonal forcing. This in turn implies maximal exchange flow (where the exchange is only controlled by the stratification and the strait dimensions). A different situation arises in M90: The exchange flux, which exhibits a two-layer pattern year round, has the same seasonal pattern as the PD in terms of the minimum and maximum of the flux. This may indicate that the depth of the interface at the Gulf of Aden is still important during the summer months; thus the exchange flux is reduced relative to the winter months, and the flow is submaximal. Transition to maximal exchange flow as a consequence of sea level reduction was also predicted by Siddall *et al.* [2002, 2004], and further discussion of the issue can be found in those papers.

[15] The model results indicate that mixing at the strait is intensified as the sea level is reduced: The salinities of the Gulf of Aden are almost fixed around a value of ~36 psu but are enriched via the entrainment process along the strait, exhibiting a seasonal pattern similar to that of the Red Sea outflow water (RSOW) when reaching the Hanish Sill (for example, Figures 1a, 1d, 1g, and 1j). Properties such as salinity and the temperature of the RSOW during the sea level reduction experiments reveal a seasonal pattern, which did not appear at the PD. The seasonal pattern of the temperature field can be attributed to the seasonal pattern of temperatures at the Gulf of Aden, which affects the RSOW layers by mixing and thus shows high temperature values in summer compared to winter.

2.3. Salinity

[16] As expected, the salinity field is characterized by dramatic changes as the sea level is reduced. As a consequence of increasing basin isolation and the high evapora-

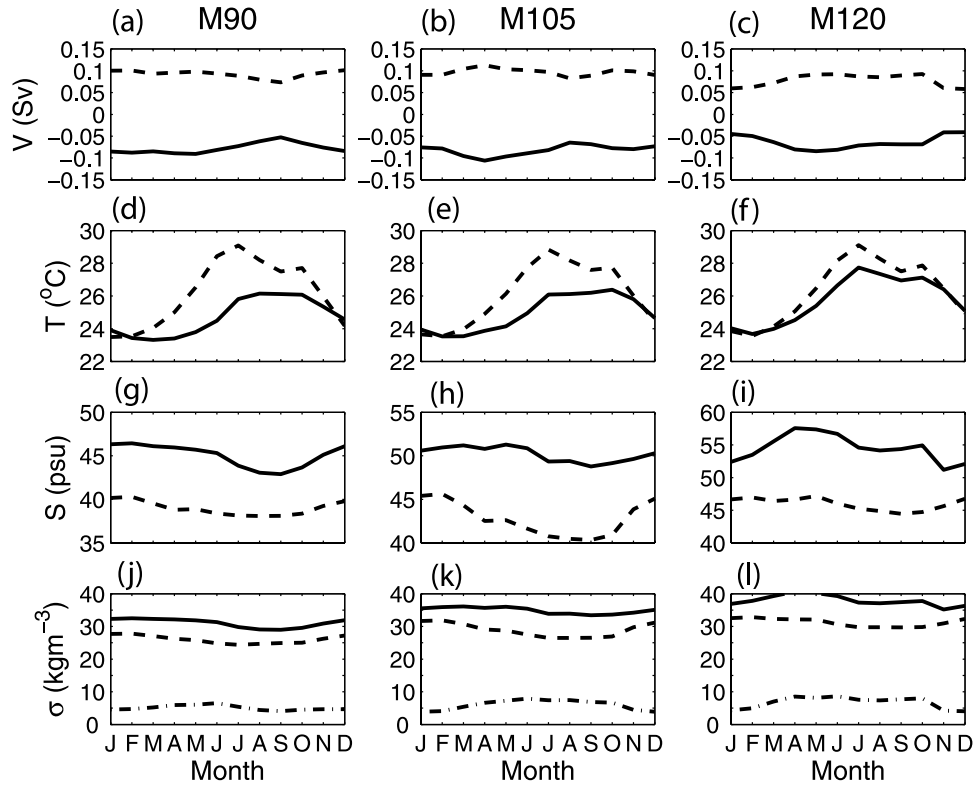


Figure 1. Monthly average exchange properties at the Hanish Sill. Left to right columns depict local sea level reduction of 90 m (M90), 105 m (M105), and 120 m (M120). From top to bottom are exchange flux, temperature (T), salinity (S), and potential density anomaly (σ). The solid line represents the Red Sea (RS) outflow water, and the dashed line represents the incoming Gulf of Aden (GA) surface water. The evolution of the exchange pattern from submaximal at M90 (closer to the present-day simulation, see Figure S7 in the supplementary information) to the maximal exchange flow at M120 can be seen, where the exchange rate is dominated by stratification and the dimensions of the strait. The dash-dotted line at the bottom subplot at each column presents the stratification, which is the subtraction of the density between the two layers. Note that the salinity values have a different scale in the three different plots.

tion rate, the annual average salinity field is increased from ~ 40.5 psu for the PD to ~ 46.7 psu at M90, to ~ 54.7 psu at M105, and to ~ 67.9 psu at M120 (Figure 2). Interestingly, although the average exchange flux at the strait at M90 is reduced dramatically to $\sim 24\%$ of its value for the PD simulation, an increase of 6 psu is observed. In comparison, while the exchange flux in M120 is reduced to 19% of its value for PD, a ~ 27 psu difference in the average salinity occurs. The high sensitivity of the basin to sea level reduction can be partially explained by the relative importance of the evaporation flux (from the whole RS surface) compared to the flux entering the strait. As the sea level is reduced, the fluxes entering the strait are reduced, and thus the relative importance of the evaporation flux increases (although the evaporation flux is reduced when the sea level is reduced because of the decrease in RS surface area), and so the sensitivity to mixing and sea level reduction increases. This fact may be easily demonstrated by combining volume and salt conservation at the strait cross section to evaluate the RS salinity at steady state, which gives $S_{RS} = S_{GA}Q/(Q - E)$, where S_{RS} is the RS salinity,

S_{GA} is the salinity of the water entering from the Gulf of Aden, Q is the flux entering the RS, and E is the net evaporation flux. The net evaporation flux (E) is 0.03 sverdrups (Sv) ($1 \text{ Sv} = 10^6 \text{ m}^3 \text{ s}^{-1}$) at present (calculated by using the RS surface area and evaporation rate of 2 m a^{-1}); assuming that the evaporation rate at LGM was the same, this value is reduced by approximately half (as a result of the reduced surface area during LGM), which is compared with 0.37 Sv for Q at present and just 0.06 Sv for a local sea level reduction of 120 m. However, using the fluxes evaluated from our model results and $S_{GA} = 37$ psu results in much lower salinity values compared to our model results for the reduced sea level experiment (e.g., 44.8 psu and 48.5 psu for the experiments M105 and M120, respectively) and very similar salinity results on average for the PD experiments (40.3 psu compared with 40.5 psu in the PD simulation). These results suggest that additional factors contribute to the higher sensitivity to sea level reduction delivered by our model. The reason for the relative salinity differences between the experiments and simple salinity balance calculations is an increase in sensitivity to the

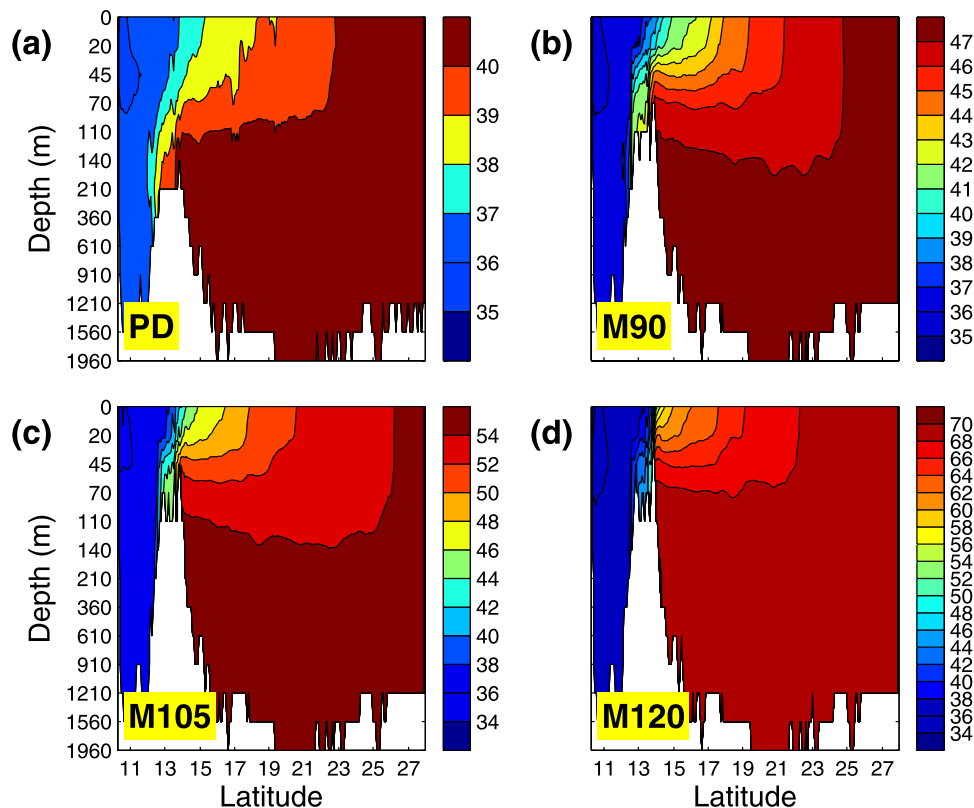


Figure 2. Annual zonally averaged salinity along the central axis as a function of sea level reduction for (a) present day, (b) -90 m, (c) -105 m, and (d) -120 m. Note that the depth scale is not linear. The volume-averaged salinities are 40.5 psu, 46.7 psu, 54.7 psu, and 67.9 psu, correspondingly.

mixing process at the strait as the sea level is reduced, as will be discussed in section 3.

[17] As local sea level is decreased, the S-N sea surface salinity gradient increases. The largest increase occurs at the southern part because of the exchange flux, with a more moderate increase from the central RS to its northern tip. Thus sea surface salinity changes from ~ 37 psu at Perim to 43, 50, and 63 psu at 17°N latitude and reaches 46, 55, and 69 psu at the northern tip for M90, M105, and M120, respectively. In comparison, a steady S-N salinity gradient is observed in PD (Figure 2, top left). At depth, all experiments show relatively homogeneous salinity values with 40.75, 47.2, 54.5, and 69.5 psu for the PD, M90, M105, and M120 simulations, respectively. Clearly, our model salinity values for the reduction of 120 m (i.e., M120) are much higher than the available estimates for the salinity field during LGM, on the basis of sediment records (48.6–57 psu [Arz *et al.*, 2003; Hemleben *et al.*, 1996; Reiss *et al.*, 1980; Lock and Thunell, 1988; Geiselhart, 1998]). The salinity field of M105 is the one that best fit these estimates. A full discussion on this topic will be given in section 3.

2.4. LGM Experiments

[18] In order to obtain estimates of the atmospheric conditions during LGM employed for experiments M120L and M105L, we used results taken from experiments based upon the use of an atmospheric general circulation model

(AGCM) to reconstruct both LGM and present-day conditions as a reference [Collins *et al.*, 2006; Otto-Bliesner *et al.*, 2006]. The AGCM predicts a general increase (as high as 30%) in the annually averaged wind strength during LGM compared to the simulated present day values (this result agrees with the previously published result for LGM by Peltier and Solheim [2004]). Since the present-day average values are ~ 5 m s^{-1} , the winds during LGM are ~ 7 m s^{-1} on the average, consistent with the wind strength suggested by Rohling [1994]. The resolution of the AGCM cannot capture the orographic effect of the mountains surrounding the RS, and the wind is not directed along the RS main axis for either the present-day or LGM simulations. However, we assume that orographic steering was at least as strong when the sea level was reduced as during the present day; thus the direction of the wind is assumed to be directed along the main axis of the RS also during LGM. To obtain climatological, zonal, and meridional wind components for the LGM, we multiplied Da Silva *et al.*'s [1994] wind components, which were used for the PD analysis, by 0.8 at the summer months (June–September) and by a factor of 1.4 for the rest of the year to simulate reduced SW monsoons at the summer and intensified winter NE monsoons, consistent with the available literature (section 1 and references therein). The present-day specific humidity was multiplied by a factor of 0.75, and 4°C was subtracted from the present-day air temperature in order to set

a climatological forcing consistent with the AGCM results. The incoming shortwave radiation chosen is unchanged and has the same values as for present-day simulation, in agreement with the AGCM results, which are characterized by a negligible reduction of insolation during LGM compared to the present-day values, and with a previous estimate [Prell, 1984]. In general, the AGCM results are also characterized by reduced precipitation at the LGM compared with the present-day results. Since the precipitation is assumed to be negligible even for present-day conditions relative to the evaporation rate, no changes have been made for the assumed precipitation. The temperature and salinity changes during the LGM at the buffer zone, within the Gulf of Aden, are somewhat uncertain. In this buffer zone the hydrography of *Levitus and Boyer* [1994] for the present-day data has been modified in order to simulate the open ocean conditions during LGM: We subtracted 2°C from the temperature profile (according to *CLIMAP Project Members* [1981], *Thunell et al.* [1988], *Pothuri and Malmgren* [2005], *Cayre and Bard* [1999], and *Rostek et al.* [1997]) and added 1 psu to the salinity profile in order to enable us to fit the observed global salinity increase at the LGM. This is consistent with an estimated increase between ~1.5 psu [Banakar et al., 2005] and 1 psu [Anajali et al., 2005] for the eastern Arabian Sea.

2.5. Hydrography

[19] In this section our purpose is to present a test of the sensitivity of our results to atmospheric conditions, while fixing the assumed local sea level reduction. We choose to discuss only the relations between the pair of experiments M120 and M120L, since the relations between the pair of experiments M105 and M105L are similar. The atmospheric changes for M120L relative to M120 (see supplementary information for PD atmospheric conditions) can be divided into two parts:

[20] 1. The first part is atmospheric changes that mainly influence the seasonal circulation pattern, namely, an increase in the NE monsoons during the winter compared to the SW monsoon wind during summer and decreased atmospheric specific humidity (both of which increase the thermohaline forcing at winter compared to summer, hence amplifying the PD trend). The impact of changes in the seasonality of the forcing on different aspects of the RS's dynamics will not be discussed, as these are beyond the scope in this article.

[21] 2. The second part is atmospheric changes that influence the hydrographic conditions at the RS but not their seasonality or spatial distribution, i.e., air temperature (which is colder by 4°C than the present-day air temperature throughout the year) and hydrography conditions at the Gulf of Aden. The evaporation rate is characterized by higher annual average values at M120L (2.024 m a⁻¹) relative to that at M120 (1.84 m a⁻¹), a consequence of the intensified wind and the decrease in the atmosphere humidity that enables the evaporation rate to overcome the effect of reduced air temperature (which acts to reduce evaporation).

[22] Because of the above changes in atmospheric conditions, the volume and annually averaged differences in the salinity field between the experiments M120 (67.9 psu) and

M120L (70.8 psu) are slightly higher than 1 psu, the same as the difference in salinity obtained for the pair M105 (53.7 psu) and M105L (55.8 psu). Since the exchange flux at the Bab el Mandab is characterized by minor changes in the surface layer (annual averages: M120, 0.0782 Sv; M120L, 0.08 Sv), there is no additional "isolation effect," and thus 1 psu growth can be attributed to changes in salinity conditions at the Gulf of Aden between the experiments. The remaining small increase of 1–2 psu between the experiments (above 1 psu) is attributed to the higher evaporation rate at M120L (2.024 m a⁻¹) relative to M120 (1.84 m a⁻¹). This implies a minor influence of the atmospheric conditions on the salinity field compared to the effect due to the reduced sea level.

[23] The temperature field reveals the expected lower temperature for M120L (an annual volume average of 18.2°C) relative to M120 (21.83°C) because of the lower air temperature and lower temperature conditions at the Gulf of Aden. The annual distribution of the SST field (not shown) for the modified forcing condition relating to M120 is in agreement with previous estimations for SST, with a 2–4°C reduction relative to PD [*CLIMAP Project Members*, 1981; *Thunell et al.*, 1988; *Arz et al.*, 2003], possibly indicating that our forcing conditions in terms of air temperature and temperature conditions at the Gulf of Aden are relatively good.

3. Discussion

3.1. Mixing at the Strait of Bab el Mandab

[24] Assuming that the topography of the Strait of Bab el Mandab did not change significantly since the LGM, a local reduction of sea level of 120 m would have left a water column above the Hanish Sill of depth 17 m (today 137 m [Werner and Lange, 1975]) and a width of ~6 km. Under a greater sea level reduction of 135 m the exchange flow through the strait would be entirely shut down; however, the existence of species such as benthic foraminifera and pteropods during LGM points to a moderate exchange flow at that time. On the basis of our OGCM results, a 120 m sea level reduction would result in a salinity of up to 67.9 psu, on the average 10–18 psu above the available estimates. Is it possible that the salinity in the RS was this high? Could it be that the estimated salinity is biased to low values because of the uncertainties that result from the nonlinear relation between salinity and $\delta^{18}\text{O}$? Our results support the estimated value of around 55 psu.

[25] In order to test the direct effect of reduced sea level on $\delta^{18}\text{O}$, we have employed a simple isotopic model based on that described by *Rohling* [1999] and *Siddall et al.* [2003]. Using this model, we are able to demonstrate that the isotopic model predicts $\delta^{18}\text{O}$ of 7–8 ppt for a reduction of 120 m, much above the observed (section 3.2). In addition, we note that the sediment records are characterized by relatively short-duration aplanktonic zones throughout the last 500 ka of Earth history, so it is reasonable to assume that the maximum value of salinity was generally close to but slightly above the lethal salinity of about 49 psu during the aplanktonic intervals. Finally, sediment cores suggest a salinity gradient starting from 47 psu in the southern RS,

through 53 psu in the center, and up to 57 psu in the north [Fenton *et al.*, 2000; Hemleben *et al.*, 1996], in agreement with our experiment based upon the assumption of a sea level reduction of 105 m. For a local reduction of 120 m, not only does the model salinity in the northern RS reach the high level of 67.9 psu, but it also reaches 58 psu in the southern RS, far above the lethal salinity for plankton, in contrast to the existence of a continuous sedimentation record there.

[26] Assuming that maximum salinity was indeed never higher than 57 psu, there is a large discrepancy between the model and the estimated salinity values if we assume a local sea level reduction as high as 120 m. Ascribing these large differences to an error in the model would appear unreasonable: In the control experiment for present-day conditions the model predicted the salinity field reasonably well, with the largest differences compared to observations being ~ 0.5 psu at the surface of the RS and much smaller in the subsurface layers (see PD simulation for further detail in the supplementary information). In the following we will discuss the possible explanations for the discrepancies between model-predicted and reconstructed salinities. We concentrate on two possibilities: (1) uncertainties regarding atmospheric conditions during LGM, which might have been more humid and thus dramatically reduced the influence of basin isolation on the salinity field, and (2) uncertainties in the depth of the sill during LGM. We will show that the second possibility is the most likely.

[27] Concerning atmospheric properties, humid conditions at the RS are generally attributed to the SW monsoons during the summer months; however, evidence from the RS and the Arabian Sea as well as from the Gulf of Aden shows that the NE monsoons were enhanced during LGM, implying less humid conditions at the southern part of the RS (section 1 and references therein). There is suggestive evidence that could indicate higher precipitation in the northern part of the RS. At the northern tip of the Gulf of Eilat, planktonic foraminifera seem to have survived during LGM [Halicz and Reiss, 1981; Reiss *et al.*, 1980], indicating much less hostile conditions in terms of salinity values than appear in the rest of the RS, opposite to the present-day trend. Additionally, evidence from Lake Lisan, just 150 km north of the Gulf of Eilat, shows that the lake level was high at that time [Bartov *et al.*, 2002], again possibly pointing to higher precipitation and more humid conditions in this region. However, the extinction of planktonic foraminifera from sediment records at the southern part of the Gulf of Eilat [Winter *et al.*, 1983] and in the northern RS suggests that this increase in precipitation, if it existed, did not extend farther southward than the Gulf of Eilat region. Moreover, there is evidence suggesting that the present-day salinity trend, i.e., an increase of salinity from south to north, was also characteristic of LGM conditions: Geiselhart [1998], in particular, demonstrated increasing values of $\delta^{18}\text{O}$ from south to north, which may also indicate a similar salinity gradient. On the basis of several sediment records taken along the main axis of the RS, Fenton *et al.* [2000] show that the “aplanktonic zone” appeared first in the northern part of the RS and then extended southward, suggesting that

higher salinity was first established in the north, as expected if the salinity trend has not changed since that time.

[28] It is most reasonable to attribute the differences in the salinity to a marked change in basin isolation as may result from error in the depth of the water column at the strait. That it is, in fact, sea level that is the main factor controlling salinity is demonstrated by the results in experiments M120, M105, M90, and PD. In contrast, differences in the salinity values due to the variations in atmospheric conditions we employed, while leaving sea level unchanged, are relatively minor. The above discussion suggests that the exchange rate with the Gulf of Aden during LGM was significantly higher than would be expected for a local 120 m sea level reduction. The model results are in good agreement, however, with the salinity values when the sea level is reduced by only 105 m (experiments M105 and M105L), which translates to a ~ 35 m water column above the sill. It is important to note that an assumed reduction in local sea level of 120 m is the value that would be in accord with the globally averaged reduction of 135 m suggested by Lambeck *et al.* [2002] if the difference between the LGM eustatic and local decrease were to be the same 15 m, as in the ICE-5G (VM) model of Peltier [2004].

[29] Using an original approach, Siddall *et al.* [2003] estimated sea level on the basis of $\delta^{18}\text{O}$ values from the central RS and used an inviscid hydraulic model to evaluate fluxes at the strait. Siddall *et al.* [2003] assumed a maximum local sea level reduction at the LGM of 120 m and then reconstructed variations in sea level through the glacial-interglacial cycle with an estimated accuracy of 12 m, where the uncertainties are related to atmospheric conditions. Here we extend the work of Siddall *et al.* [2003] to implicitly include interfacial mixing processes due, for example, to wind stress, bottom friction, tides, etc. All these processes produce turbulent kinetic energy, which is partially converted to mixing between the layers, and thus reduces stratification and, in addition, can influence the exchange flux directly through bottom friction, shearing, and wind stress (depending on the direction of the wind in relation to the surface current direction). For given stratification and strait dimensions, if these processes were not negligible, the fluxes at the strait will be generally less than those predicted by the discrete-layered hydraulic model. Concerning the RS, the mixing between the layers and the resulting reduction of the exchange flux act to increase basin isolation, which would increase both salinity and $\delta^{18}\text{O}$ because of the effect of evaporation. Smeed [2004] discussed the influence of these processes on the validity of a hydraulic model for the present-day Strait of Bab el Mandab. Using energy considerations, he estimated that the energy transferred to mixing at the strait is on the order of 15% of the total energy flux of the overflow from the Hanish Sill (0.8 GW [Smeed, 2004]). Smeed [2004] suggested that this mixing could reduce the exchange fluxes estimated using the inviscid hydraulic model theory by 10–20%. However, he claimed that since most of the mixing occurs in the shallow regions of the strait, which are already well mixed and downstream of the sill, the exchange flux might still be assumed to be close to that predicted by the simple hydraulic model. Indeed, Siddall *et al.* [2002] succeeded

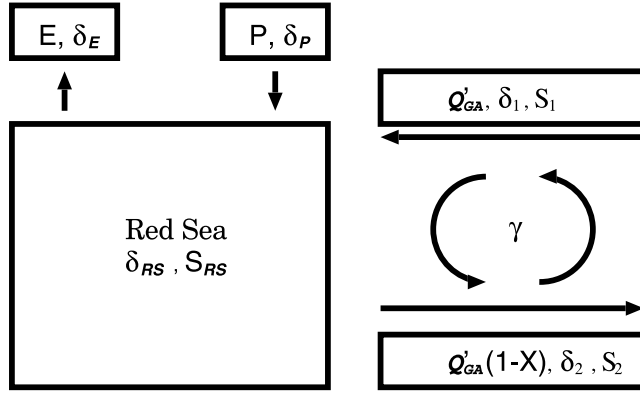


Figure 3. A scheme of the box model. The boxes simulate the RS proper and the exchange flux at the strait, where the mixing between the strait boxes is indicated by the parameter γ . The expression in the boxes indicating the different salinity and $\delta^{18}\text{O}$'s contributions after the mixing effect is included (e.g., $\delta_1 = (1 - \gamma)\delta_{GA} + \gamma\delta_{RS}$), in which a steady state solution is represented by equations (5) and (6), respectively. Here Q'_{GA} indicates the hydraulic volume flux entering the RS after correction for the mixing effect (see equation (2)), δ_{GA} and S_{GA} are the $\delta^{18}\text{O}$ and salinity values of the Gulf of Aden surface water, δ_{RS} and S_{RS} are the $\delta^{18}\text{O}$ and salinity values of the RS in average, and δ_E and δ_P are the isotopic composition of the evaporation and precipitation. P, E, and X are the precipitation, evaporation, and the net evaporation volume flux (i.e., $E - P$), respectively. Following *Siddall et al.* [2003], the atmospheric conditions driving the model are set to 2 m a^{-1} for the net evaporation and 0.7 for the relative humidity. The air temperature is assumed to decrease linearly from present values by 5°C as the sea level falls by up to 120 m.

in simulating the fluxes at the Strait of Bab el Mandab under present-day conditions, in good agreement with observations, indicating that the inviscid hydraulic model is a good approximation for current conditions as well. *Siddall et al.* [2004] (in a supplementary paper to the one by *Siddall et al.* [2003]) compared the relative importance of bottom friction and tides on the flow through the Strait of Bab el Mandab for the LGM and for the present-day simulation, pointing out that these processes are comparable in importance in both periods. Thus *Siddall et al.* [2004] suggested that because the inviscid hydraulic model for present-day conditions is in good agreement with observations while neglecting of these processes, it might still be a good approximation under reduced sea level conditions.

[30] On the basis of our results, however, we suggest that the mixing process is significantly more effective when sea level is reduced at the Strait of Bab el Mandab and therefore that it cannot be neglected (even assuming that the mixing rate, referred to here as the fraction of the water column that is mixed, was the same as the present-day mixing rate) because most of the shallow parts of the strait become exposed (and for further reasons to be discussed in section 3.2). Our results also demonstrate that although mixing processes seem insignificant so long as sea level is

not reduced by more than 100 m or so, uncertainties in the amount of mixing may still introduce an error in reconstructed relative sea level.

3.2. Hydraulic Control Model With Mixing

[31] In order to further investigate the effect of reduced sea level and of mixing at the Strait of Bab el Mandab on the properties within the RS (i.e., salinity and $\delta^{18}\text{O}_{\text{calcite}}$), we have employed a simple box model (Figure 3) which takes into account recent theoretical work concerning the influence of friction and mixing on the exchange fluxes at straits compared to the influence characteristic of the hydraulic limit (*Hogg et al.* [2001], *Ivey* [2004], among others). In the work by *Hogg et al.* [2001] it is shown that the ratio (f) of fluxes between the hydraulic control limit (no mixing occurs) and the characteristics of a fully mixed water column (defined as the diffusion limit) is given by

$$f = f(G_r A^2), \quad (1)$$

where $G_r = g'h^3/k_v^2$ is the Grashof number and $A = h/l$ is the aspect ratio of the strait. The variable l is the distance over which the velocity changes significantly as the fluid moves along the strait, h is the water column depth, g' is the reduced gravity, and k_v is the eddy viscosity coefficient for momentum. For large values of the parameter $G_r A^2$ ($>10^6$) the exchange flow reaches the hydraulic limit, and for small values of $G_r A^2$ (<40) the exchange fluxes approach the diffusion limit. For the large range of values between those two limits, f is given approximately by

$$f = 1 - 1.7(G_r A^2)^{-1/4}. \quad (2)$$

[32] In the work by *Hogg et al.* [2001] the parameter $G_r A^2$ was linked to the ratio between the interfacial mixed layer thickness (δ) and the water column height (h), leading to a simpler formula

$$f = 1 - 0.5\delta/h = 1 - \gamma, \quad (3)$$

where we have defined a dimensionless parameter $\gamma = 0.5\delta/h$ to characterize mixing efficiency, ranging from 0 to 0.5, where the lower value reflects the inviscid hydraulic limit ($\delta \rightarrow 0$) and the upper limit corresponds to the diffusive limit for which the water column is fully mixed ($\delta \rightarrow h$). *Smeed* [2004] estimated that $G_r A^2 = 2 \times 10^4$ for the present-day Strait of Bab el Mandab. Therefore according to equation (2), $f \cong 0.85$, which translates to $\gamma = 0.15$ for the present Bab el Mandab Strait.

[33] The hydraulic limit fluxes (Q_h) for reduced sea level are calculated from the surface area of the RS (S), the buoyancy flux from the RS area ($B_o = 3.1 \times 10^{-8} \text{ m}^2 \text{ s}^{-2}$ [*Finnigan et al.*, 2001]), and the physical dimensions of the strait ($b = \text{width}$, $h = \text{height}$), using the equation [see *Ivey*, 2004]

$$Q_h = 0.35h(B_o b^2 S)^{1/3}. \quad (4)$$

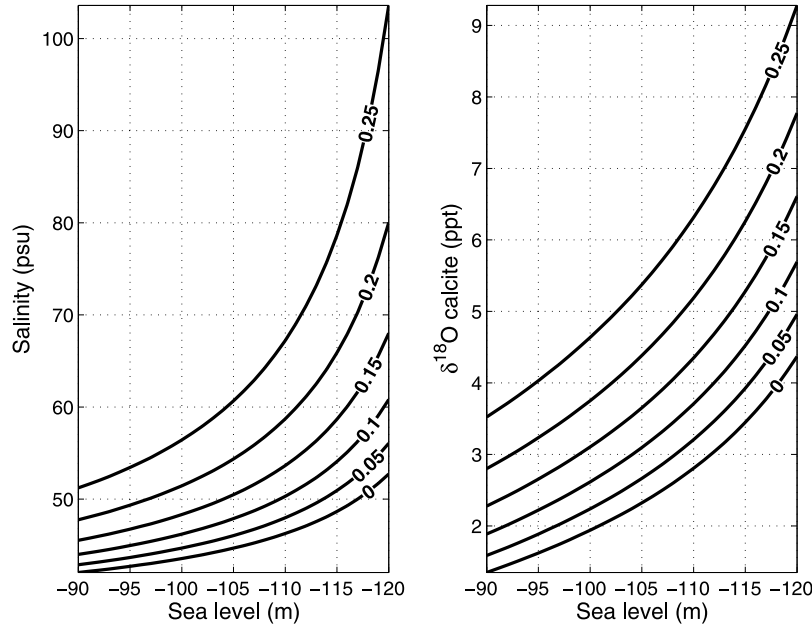


Figure 4. (left) Salinity as function of sea level, with contours indicating different relations for different values of γ ranging between 0 and 0.25, and (right) $\delta^{18}\text{O}_{\text{calcite}}$ as function of sea level as obtained by the isotopic model, with contours indicating different relations for different values of γ ranging between 0 and 0.25.

[34] The salinity for various mixing rates and locally reduced sea level between 90 m and 120 m (for which we assume a hydraulically controlled exchange flux) is shown in Figure 4 (left). The steady state solution for the RS's salinity (S_{RS}) is given by

$$S_{\text{RS}} = \frac{((1 - 2\gamma)(1 - \gamma)Q_h + X\gamma)S_{\text{GA}}}{(1 - 2\gamma)(1 - \gamma)Q_h - (1 - \gamma)X}. \quad (5)$$

Explanations of the different variables appearing in this equation will be found in the caption of Figure 3 in which the box model is described.

[35] As is evident on the basis of Figure 4, for a reduction of 120 m and for reasonable values of $\gamma \cong 0.15$, similar to current estimates of γ at the Strait of Bab el Mandab, the salinity increases to 68 psu. This value is much higher than the observed salinities estimated for LGM and is similar to the value obtained by the OGCM for M120. For a reduction of 105 m and γ somewhat above the present-day value of 0.15 (as would be expected when the water column depth is significantly shallower), the salinity is 50–55 psu, as suggested in other studies [Fenton *et al.*, 2000; Arz *et al.*, 2003; Hemleben *et al.*, 1996; Reiss *et al.*, 1980; Lock and Thunell, 1988; Geiselhart, 1998].

[36] Most of the salinity estimations are based on the present-day linear relation between $\delta^{18}\text{O}_{\text{calcite}}$ and the salinity, which may not hold for the past [Siddall *et al.*, 2004; Rohling, 1994]. We therefore employ a simple isotopic model that has already been used for the Mediterranean Sea [Rohling, 1999] and for the RS [Siddall *et al.*, 2003], for which we have already included the influence of mixing

processes at the strait (Figure 3). The steady state solution for the RS $\delta^{18}\text{O}$ value (δ_{RS}) is given by

$$\delta_{\text{RS}} = \frac{((1 - 2\gamma)(1 - \gamma)Q_h + X\gamma)\delta_{\text{GA}} - X\delta_E}{(1 - 2\gamma)(1 - \gamma)Q_h - (1 - \gamma)X}. \quad (6)$$

[37] This equation reduces to the similar equation employed by Rohling [1999] in the absence of mixing (i.e., $\gamma = 0$). As in the work by Rohling [1994] we have also assumed that for the RS, $E\delta_E - P\delta_P \approx X\delta_E$ as $P \ll E$ is a good approximation for this basin. The $\delta^{18}\text{O}$ values for the Gulf of Aden water entering the RS (δ_{GA}) have been corrected for continental ice sheet growth by increasing the $\delta^{18}\text{O}$ value by 0.012 ppt per meter sea level fall [Fairbanks, 1989] with respect to the present values (0.1 ppt [Ganssen and Kroon, 1991]). Following Siddall *et al.* [2003], the atmospheric conditions driving the model are set to 2 m a^{-1} for the net evaporation and 0.7 for the relative humidity. The air temperature is assumed to decrease linearly from present values by 5°C as the sea level falls by up to 120 m. Using this isotopic model, the $\delta^{18}\text{O}_{\text{calcite}}$ was calculated for the range of 90–120 m of sea level fall (see Rohling [1999] for further details of the isotopic model).

[38] The results for different values of γ are presented in Figure 4 (right). As expected, there is a high sensitivity of $\delta^{18}\text{O}_{\text{calcite}}$ to sea level reduction and for increasing values of γ , similar to the box model results for the salinity values. Our results for $\gamma = 0$, the hydraulic limit, are almost identical to the results of Siddall *et al.* [2004, Figure 4b] (bold dashed line). For a sea level reduction of 120 m a value of ~ 0.15 for γ (which is very likely a lower limit for the reduced sea level cases) is translated to a change of

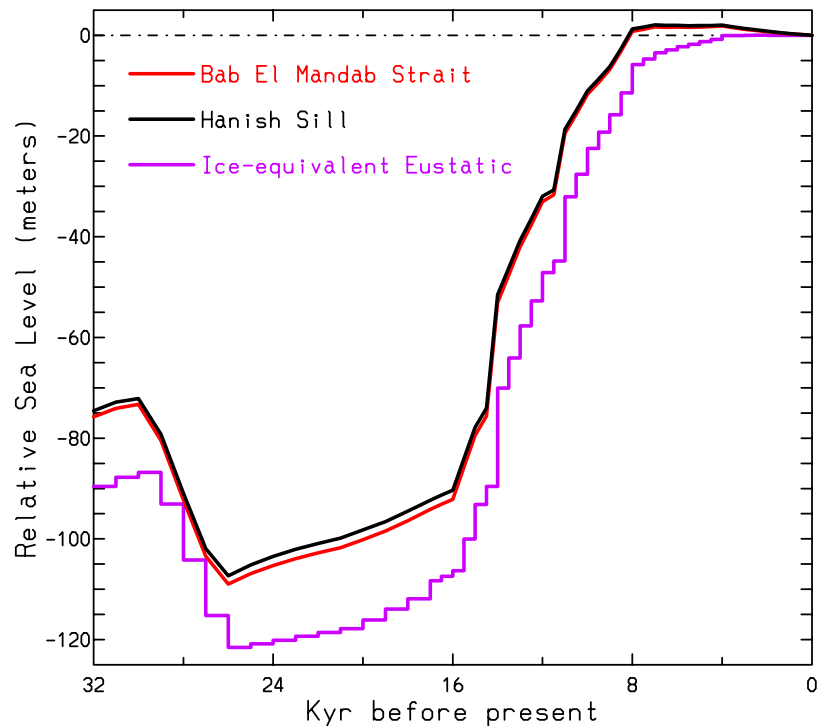


Figure 5. Relative sea level history prediction based on the ICE-5G (VM2) model [Peltier, 2004] for two closely spaced locations in the Strait of Bab el Mandab region, when the assumed modern level is zero. For comparison purposes these two local time series are shown together with the ice equivalent eustatic sea level history of the same ICE-5G (VM2) model.

~ 6.6 ppt, much higher than the observed values during the LGM, which are closer to ~ 4.3 ppt. Values of 4.3 ppt for $\delta^{18}\text{O}_{\text{calcite}}$ are translated to a sea level reduction of 104 m for $\gamma = 0.175$. This value for γ was also estimated on the basis of our box model results and reconstructed salinity during LGM within the range of 50–57 psu based on sediment records. This local sea level reduction is translated to local relative sea level at the Hanish Sill of 33 ± 10.75 m, where the ± 10.75 m uncertainty is due to our uncertainties in atmospheric conditions and in the strength of the mixing processes in the strait (i.e., as represented by the γ value). We assume ± 0.025 to be the uncertainty in the γ value, which translates to ± 3 m (ranges between 0.15 and 0.2). Additional sensitivity tests to changes in the different driving forces [cf. Siddall *et al.*, 2004] have led to attributed errors as follows: ± 3 m for our uncertainties in the net evaporation (ranges between 1.8 m a^{-1} and 2.2 m a^{-1}), ± 2.5 m for our uncertainties in the relative humidity (0.6–0.8), and ± 1.25 m due to uncertainties in temperature (with temperature uncertainties in the range of $\pm 2^\circ\text{C}$). Additional uncertainty of ± 1 m is due to ± 0.1 ppt uncertainty in $\delta^{18}\text{O}$ measurements.

[39] Our results show that only for extremely low net evaporation conditions of 1 m a^{-1} (and a conservative value of γ changes between 0.15 and 0.2), could the local sea level reduction based upon the isotopic model be as large as 120 m while still fitting the observed $\delta^{18}\text{O}$ and salinity characteristic of the LGM. Such low net evaporation,

however, is inconsistent with the previous estimation of 2 m a^{-1} [Rohling, 1994]; our estimation of 2 m a^{-1} based on the OGCM simulated LGM conditions (section 2.5), with evidence pointing to less humid conditions at the RS during the LGM (section 1 and references therein), suggesting net evaporation flux close to or above the present values.

3.3. ICE-5G (VM2) Model of Deglaciation and Postglacial Sea Level History

[40] The ICE-5G (VM2) model of the most recent global deglaciation event of the Late Pleistocene ice age [Peltier, 2004] is a model specifically designed as a vehicle with which to understand the space-time-dependent history of relative sea level change caused by the meltback of the significant accumulations of land ice that existed at LGM. It is the most recent product of a series of increasingly more accurate models of these processes [Peltier, 1994, 1996, 2004; Peltier and Andrews, 1976; Wu and Peltier, 1982; Tushingham and Peltier, 1991]. This model is characterized by a significant redistribution of Northern Hemisphere ice from the Eurasian sector to the North American continent, a modification required by several lines of new evidence, including the geomorphology-based inferences of the distribution of glacial maximum land ice in Eurasia produced by the European Quaternary Environment of the Eurasian North project [Svensen *et al.*, 2003] and by space-geodetic measurements of the vertical motion of the crust in North America [Argus *et al.*, 1999; Lambert *et al.*, 2001].

[41] From the perspective of the present focus of refining the interpretation of the RS salinity record in terms of the sea level change that occurred at the location of the Hanish Sill in the Strait of Bab el Mandab, it is necessary to distinguish between the LGM ice equivalent eustatic level of ~ 120 m and the level that existed locally at this time. Figure 5 shows the relative sea level history prediction for two closely spaced locations in the target area relative to an assumed modern level of zero. For the first site, which we will refer to simply as the Bab el Mandab Strait (Figure 5), the model predicts that sea level was lower at 21 ka by 101.5 m and at 26 ka by 108.5 m. The equivalent prediction for the location of the Hanish Sill itself (Figure 5) is that at 21 ka sea level was lower by 99.6 m and at 26 ka by 106.9 m. We present the results for 26 ka as well as for the conventional LGM age of 21 ka, as it has been suggested by *Peltier and Fairbanks* [2006] that LGM could have occurred some 5 ka earlier than has conventionally been assumed.

[42] Since the modern depth of the water column over the Hanish Sill is ~ 137 m, our results clearly imply that at 21 ka the depth of the water column there should have been ~ 37.4 m. However, if the salinity inference for the RS is actually the inference for LGM, and if LGM were to have occurred at 26 ka rather than 21 ka, then our results are predicting a depth of the water column over the sill of 30.1 m. Taking this possible timing error into account, our prediction might best be expressed as the mean of these two results, or 33.75 ± 3.65 m. This result is very close indeed to that inferred on the basis of our RS salinity and $\delta^{18}\text{O}$ analysis.

4. Conclusion

[43] Our main conclusion based on the model results is that the exchange rate during the LGM was considerably

higher than would be expected with a local sea level reduction of 120 m, whereas it is in good agreement with a drop of 104 ± 10.75 m. This estimate for the local sea level reduction is equivalent to a 33 ± 10.75 m water column depth above the Hanish Sill at LGM, where the uncertainties of ± 10.75 m are due to our estimated uncertainties in atmospheric conditions and in the mixing parameter γ (see section 3.2). This result is very close to the prediction of 33.75 ± 3.65 m based on the ICE-5G (VM2) model. The isotopic model results also point to the need for an accurate estimate of mixing intensity in order to reconstruct sea level on the basis of sediment records, as changes of 10 m or more are obtained for a given value of $\delta^{18}\text{O}_{\text{calcite}}$ (e.g., 3 ppt) and γ between 0 and 0.15. The current analysis also supports previous estimation of 53 ± 4 psu for the salinity values of the RS during LGM. The upper limit of 57 psu is based on our OGCM results for the S-N salinity gradient and constraints set by the continuous sediment record at the southern part of the RS. The lower limit of 49 psu is due to the existence of “aplanktonic zone” in sediment record in most places of the RS during the LGM.

[44] **Acknowledgments.** We would like to thank Mark Siddall, Eelco Rohling, Alon Shepon, Yosef Ashkenazi, Ahuva Almogi-Labin, and Eli Tziperman for most useful comments and discussions. However, the content of this manuscript may not necessarily represent their personal opinions of the matters discussed. We are grateful to Cecilia Bitz for the AGCM results; CCSM3 integrations were conducted at the National Center for Atmospheric Research (NCAR). NCAR is supported by the National Science Foundation. This research was supported by the Israel Science Foundation (grant 781/04 to H.G.) and by NSERC grant A9621 to W.R.P. The work at Toronto is also a contribution to the Polar Climate Stability Network, which is funded by the Canadian Foundation for Climate and Atmospheric Science and by a Consortium of Canadian Universities. E.B. is partially supported by a Rieger Fellowship.

References

- Almogi-Labin, A., C. Hemleben, and D. Meischner (1998), Carbonate preservation and climatic changes in the central Red Sea during the last 380 kyr as recorded by pteropods, *Mar. Micropaleontol.*, **33**, 87–107.
- Almogi-Labin, A., G. Schmiedl, C. Hemleben, R. Siman-Tov, and D. Meischner (2000), The influence of the NE winter monsoon on productivity changes in the Gulf of Aden, NW Arabian Sea, during the last 530 ka as recorded by foraminifera, *Mar. Micropaleontol.*, **40**, 295–319.
- Anajali, R. C., V. K. Banakar, and T. Oba (2005), Past 100 ky surface salinity-gradient response in the eastern Arabian Sea to summer monsoon variation recorded by $\delta^{18}\text{O}$ of *G. sacculifer*, *Global Planet. Change*, **47**, 135–142.
- Anderson, D. M., and W. L. Prell (1993), A 300 kyr record of upwelling off Oman during the late Quaternary: Evidence of the Asian southwest monsoon, *Paleoceanography*, **8**, 193–208.
- Argus, D. F., W. R. Peltier, and M. M. Watkins (1999), Glacial isostatic adjustment observed using very long baseline interferometry and satellite laser ranging geodesy, *J. Geophys. Res.*, **104**, 29,077–29,094.
- Arz, H. W., J. Patzold, P. J. Muller, and M. O. Moammar (2003), Influence of Northern Hemisphere climate and global sea level rise on the restricted Red Sea marine environment during termination I, *Paleoceanography*, **18**(2), 1053, doi:10.1029/2002PA000864.
- Arz, H. W., F. Lamy, A. Ganopolski, N. Nowaczyk, and J. Patzold (2007), Dominant Northern Hemisphere climate control over millennial-scale glacial sea-level variability, *Quat. Sci. Rev.*, **26**, 312–321.
- Banakar, V. K., T. Oba, A. R. Chodankar, T. Kuramoto, M. Yamamoto, and M. Minagawa (2005), Monsoon related changes in sea surface productivity and water column denitrification in the Eastern Arabian Sea during the last glacial cycle, *Mar. Geol.*, **219**, 99–108.
- Bartov, Y., M. Stein, Y. Enzel, A. Agnon, and Z. Reches (2002), Lake level and sequence stratigraphy of Lake Lisan, the late Pleistocene precursor of the Dead Sea, *Quat. Res.*, **57**, 9–21.
- Bigg, G. R., and D. Jiang (1993), Modeling the late Quaternary Indian Ocean circulation, *Paleoceanography*, **8**, 23–46.
- Cayre, O., and E. Bard (1999), Planktonic foraminiferal and alkenone records of the last deglaciation from the eastern Arabian Sea, *Quat. Res.*, **52**, 337–342.
- CLIMAP Project Members (1981), Seasonal reconstructions of the Earth's surface at the Last Glacial Maximum, *Map Chart Ser. MC-36*, Geol. Soc. Am., Boulder, Colo.
- Collins, W., et al. (2006), The community climate system model, version 3, *J. Clim.*, **19**, 2122–2143.
- Da Silva, A., A. C. Young, and S. Levitus (1994), Atlas of Surface Marine Data 1994, vol. 1, Algorithms and Procedures, *NOAA Atlas NESDIS 6*, U. S. Dep. of Commer., Washington, D. C.
- Fairbanks, R. G. (1989), A 17000 year glacio eustatic sea level record: Influence of glacial melting rates on the Younger-Dryas event and deep-ocean circulation, *Nature*, **342**, 637–642.
- Fenton, M., S. Geislerhart, E. J. Rohling, and C. Hemleben (2000), Aplanktonic zones in

- the Red Sea, *Mar. Micropaleontol.*, **40**, 277–294.
- Finnigan, T. D., K. B. Winters, and G. N. Ivey (2001), Response characteristics of a buoyancy-driven sea, *J. Phys. Oceanogr.*, **31**, 2721–2736.
- Ganssen, G., and D. Kroon (1991), Evidence for Red Sea surface circulation from oxygen isotopes of modern surface waters and planktonic foraminiferal tests, *Paleoceanography*, **6**, 73–82.
- Geisellhart, S. (1998), Late Quaternary paleoceanographic and paleoclimatologic history of the Red Sea during the last 380,000 years: Evidence from stable isotopes and faunal assemblages, Ph.D. thesis, Inst. fur Geowiss, Tubingen, Germany.
- Goudie, A. S., B. Allchin, and K. T. M. Hedge (1973), The former extensions of Great Indian Desert, *Geogr. J.*, **139**, 243–257.
- Griffies, S., M. Harrison, R. Pacanowski, and A. Rosati (2004), A technical guide to MOM4, *Tech. Rep. 5*, NOAA/Geophys. Fluid Dyn. Lab., Princeton, N. J.
- Halicz, E., and Z. Reiss (1981), Palaeoecological relations of foraminifera in a desert enclosed sea: The Gulf of Aqaba, *Mar. Ecol.*, **2**, 15–34.
- Hemleben, C., D. Melschner, R. Zahn, A. Almogi-Labin, H. Erlenkeuser, and B. Hiller (1996), Three hundred eighty thousand year long stable isotope and fauna records from the Red Sea: Influence of global sea level change on hydrography, *Paleoceanography*, **11**, 147–156.
- Hogg, A. M., G. N. Ivey, and K. B. Winters (2001), Hydraulics and mixing in controlled exchange flow, *J. Geophys. Res.*, **106**, 959–972.
- Ivey, G. N. (2004), Stratification and mixing in sea straits, *Deep Sea Res.*, **51**, 441–453.
- Knudsen, M. (1900), Ein hydrographischer lehrsatze, *Ann. Hydr. Mar. Meteorol.*, **28**, 316–320.
- Lambeck, K., Y. Yokoyama, A. Purcell, and P. Johnston (2002), Reply to the comment by W. R. Peltier “Comments on the paper of Yokoyama et al. (2000) entitled ‘Timing of the Last Glacial Maximum from observed sea level minima’”, *Quat. Sci. Rev.*, **21**, 415–418.
- Lambert, A., N. Courtier, G. S. Sasagawa, F. Klopping, and D. Winster (2001), New constraints on Laurentide postglacial rebound from absolute gravity measurements, *Geophys. Res. Lett.*, **28**, 2109–2112.
- Large, W. G., and S. Pond (1981), Open ocean momentum flux measurements in moderate to strong winds, *J. Phys. Oceanogr.*, **11**, 324–336.
- Large, W. G., and S. Pond (1982), Sensible and latent heat flux measurements over the ocean, *J. Phys. Oceanogr.*, **12**, 464–482.
- Large, W., J. McWilliams, and S. Doney (1994), Oceanic vertical mixing: A review and a model with a nonlocal boundary-layer parameterization, *Rev. Geophys.*, **32**, 363–403.
- Levitus, S., and T. Boyer (1994), *World Ocean Atlas 1994*, vol. 4, *Temperature*, NOAA Atlas NESDIS 4, U. S. Dep. of Commer., Washington, D. C.
- Lock, S. M., and R. C. Thunell (1988), Palaeoceanographic record of the last glacial-interglacial cycle in the Red Sea and Gulf of Aden, *Palaeogeogr. Palaeoclimatol. Palaeoecol.*, **64**, 163–187.
- Marshall, J., C. Hill, L. Perelman, and A. Adcroft (1997a), Hydrostatic, quasi-hydrostatic, and nonhydrostatic ocean modeling, *J. Geophys. Res.*, **102**, 5733–5752.
- Marshall, J., C. Hill, L. Perelman, and A. Adcroft (1997b), A finite-volume, incompressible Navier Stokes model for studies of the ocean on parallel computers, *J. Geophys. Res.*, **102**, 5753–5766.
- Otto-Bliessner, B. L., E. C. Brady, G. Clauzet, R. Tomas, S. Levis, and Z. Kothavala (2006), Last Glacial Maximum and Holocene climate in CCSM3, *J. Clim.*, **19**, 2526–2544.
- Peltier, W. R. (1994), Ice age paleotopography, *Science*, **265**, 195–201.
- Peltier, W. R. (1996), Mantle viscosity and ice age ice sheet topography, *Science*, **273**, 1359–1364.
- Peltier, W. R. (2002), On eustatic sea level history, Last Glacial Maximum to Holocene, *Quat. Sci. Rev.*, **21**, 377–396.
- Peltier, W. R. (2004), Global glacial isostasy and the surface of the ice-age Earth: The ICE-5G (VM2) model and GRACE, *Annu. Rev. Earth Planet. Sci.*, **32**, 111–149.
- Peltier, W. R., and J. T. Andrews (1976), Glacial isostatic adjustment I: The forward problem, *Geophys. J. R. Astron. Soc.*, **46**, 605–646.
- Peltier, W. R., and R. G. Fairbanks (2006), Global glacial ice volume and Last Glacial Maximum duration from an extended Barbados sea level record, *Quat. Sci. Rev.*, **25**, 3322–3337.
- Peltier, W., and L. Solheim (2004), The climate of the Earth at Last Glacial Maximum: Statistical equilibrium state and a mode of internal variability, *Quat. Sci. Rev.*, **23**, 335–357.
- Plahn, O., B. Baschek, T. H. Badewien, M. Walter, and M. Rhein (2002), Importance of the Gulf of Aqaba for the formation of bottom water in the Red Sea, *J. Geophys. Res.*, **107**(C8), 3108, doi:10.1029/2000JC000342.
- Pothuri, D. N., and B. A. Malmgren (2005), Seasonal sea surface temperature contrast between the Holocene and last glacial period in the western Arabian Sea (Ocean Drilling Project Site 723A): Modulated by monsoon upwelling, *Paleoceanography*, **20**, PA1004, doi:10.1029/2004PA001078.
- Prell, W. L. (1984), Monsoonal climate of Arabian Sea during the late Quaternary: A response to changing solar radiation, in *Milankovitch and Climate*, Part I, pp. 349–366, Springer, New York.
- Reiss, Z., B. Luz, A. Almogi-Labin, E. Halicz, A. Winter, and M. Wolf (1980), Late Quaternary paleoceanography of the Gulf of Aqaba (Elat), Red Sea, *Quat. Res.*, **14**, 294–308.
- Rohling, E. J. (1994), Glacial conditions in the Red Sea, *Paleoceanography*, **9**, 653–660.
- Rohling, E. J. (1999), Environmental control on Mediterranean salinity and $\delta^{18}\text{O}$, *Paleoceanography*, **14**, 706–715.
- Rohling, E. J., M. Fenton, F. J. Jorissen, P. Bertrand, G. Ganssen, and J. P. Caulet (1998), Magnitudes of sea-level lowstands of the past 500,000 years, *Nature*, **394**, 162–165.
- Rostek, F., E. Bard, L. Beaufort, C. Sonzogni, and G. Ganssen (1997), Sea surface temperature and productivity records for the past 240 kyr in the Arabian Sea, *Deep Sea Res.*, **44**, 1461–1480.
- Siddall, M., D. Smeed, S. Matthiesen, and E. Rohling (2002), Modelling the seasonal cycle of the exchange flow in Bab el Mandab (Red Sea), *Deep Sea Res.*, **49**, 1551–1569.
- Siddall, M., E. J. Rohling, A. Almogi-Labin, C. Hemleben, D. Melschner, I. Schmelzer, and D. A. Smeed (2003), Sea-level fluctuations during the last glacial cycle, *Nature*, **423**, 853–858.
- Siddall, M., D. A. Smeed, C. Hemleben, E. J. Rohling, I. Schmelzer, and W. R. Peltier (2004), Understanding the Red Sea response to sea level, *Earth Planet. Sci. Lett.*, **225**, 421–434.
- Singh, G., R. Joshi, and A. B. Singh (1972), Stratigraphic and radiocarbon evidence for the age development of three salt lake deposits in Rajasthan, India, *Quat. Res.*, **2**, 496–505.
- Sirocko, F., M. Sarnthein, H. Erlenkeuser, H. Lange, M. Arlund, and J. C. Duplessy (1993), Century-scale events in monsoonal climate over the past 24,000 years, *Nature*, **364**, 322–324.
- Smeed, D. A. (2004), Exchange through the Bab el Mandab, *Deep Sea Res.*, **51**, 455–474.
- Svensen, J. I., V. Gataullin, J. Mangerud, and K. Polyak (2003), *Quaternary Glaciations—Extent and Chronology*, vol. 1, Elsevier, Amsterdam.
- Ten Haven, H. L., and D. Kroon (1991), Late Pleistocene sea surface temperature variations off Oman as revealed by the distribution of long-chain alkenones, *Proc. Ocean Drill. Program Sci. Results*, **117**, 445–450.
- Thunell, R. C., S. M. Locke, and D. F. Williams (1988), Glacio-eustatic sea-level control on Red Sea salinity, *Nature*, **334**, 601–604.
- Tushingham, A. M., and W. R. Peltier (1991), ICE-3G: A new global model of late Pleistocene deglaciation based upon geophysical predictions of postglacial relative sea level change, *J. Geophys. Res.*, **96**, 4497–4523.
- Van Campo, E., and J. C. Duplessy (1982), Climatic conditions deduced from 150-kyr oxygen isotope–pollen record from the Arabian Sea, *Nature*, **296**, 56–59.
- Werner, F., and K. Lange (1975), A bathymetry survey of the sill area between the Red Sea and Gulf of Aden, *Geol. Jahrb. D.*, **13**, 25–30.
- Winter, A., A. Almogi-Labin, Y. Erez, E. Halicz, B. Luz, and Z. Reiss (1983), Salinity tolerance of marine organisms deduced from Red Sea Quaternary record, *Mar. Geol.*, **53**, 17–22.
- Wu, P., and W. R. Peltier (1982), Viscous gravitational relaxation, *Geophys. J. R. Astron. Soc.*, **70**, 435–485.
- Yokoyama, Y., K. Lambeck, P. D. Deckker, P. Johnston, and L. Fifield (2000), Timing of the Last Glacial Maximum from observed sea-level minima, *Nature*, **406**, 713–716.

E. Biton and H. Gildor, Department of Environmental Sciences and Energy Research, Weizmann Institute of Science, Rehovot 76100, Israel. (hezi.gildor@weizmann.ac.il)

W. R. Peltier, Department of Physics, University of Toronto, Toronto, ON, Canada. M5S 1A7.